

ForestTrav: Accurate, Efficient and Deployable Forest Traversability Estimation for Autonomous Ground Vehicles

Fabio Ruetz^{1,2}, Nicholas Lawrance², Emili Hernández³, Paulo Borges², Thierry Peynot¹

Abstract—Autonomous navigation in unstructured vegetated environments remains an open challenge. To successfully operate in these settings, ground vehicles must assess the traversability of the environment and determine which vegetation is pliable enough to push through. In this work, we propose a novel method that combines a high-fidelity and feature-rich 3D voxel representation while leveraging the structural context and sparseness of sparse convolutional neural networks (SCNNs) to assess traversability estimation (TE) in densely vegetated environments. The proposed method is thoroughly evaluated on an accurately-labeled real-world data set that we provide to the community. It is shown to outperform state-of-the-art methods by a significant margin (0.59 vs. 0.39 MCC score at 0.1m voxel resolution) in challenging scenes and to generalize to unseen environments. In addition, the method is economical in the amount of training data and training time required: a model is trained in minutes on a desktop computer. We show that by exploiting the context of the environment, our method can use different feature combinations with only limited performance variations. For example, our approach can be used with lidar-only features, whilst still assessing complex vegetated environments accurately, which was not demonstrated previously in the literature in such environments. In addition, we propose an approach to assess a traversability estimator’s sensitivity to information quality and show our method’s sensitivity is low.

I. INTRODUCTION

Autonomous navigation in unstructured vegetated environments is essential for many robotics applications but remains an open challenge due to the non-rigid nature of vegetation and the need to consider what a ground robot can push or pass through. Forests are one such example, they are often cluttered, complex, and have occlusions and degradation of sensory information. Strategies to perform traversability estimation (TE) in such environments range from reliance on a single image to 3D probabilistic voxel maps [1], [2], [3], [4].

Single-image appearance-based TE methods are adequate for many tasks (e.g. following gravel roads with vegetation and navigating greenhouses). They can leverage high-fidelity information contained in images in combination with strong assumptions about the environments [1], [4]. However, these methods can only assess the next step locally and are

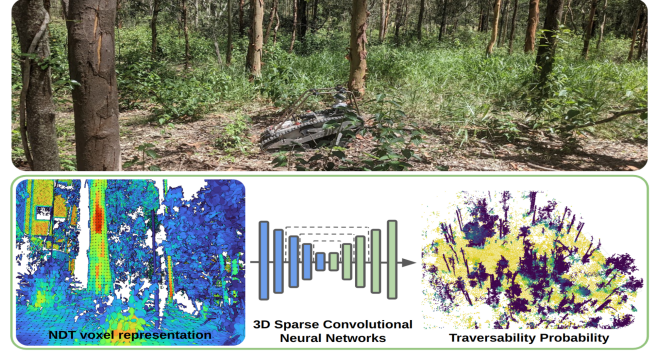


Fig. 1. Top: robot navigating in forest with low to dense vegetation. Bottom: proposed method. Features from a probabilistic 3D voxel map are passed to a sparse convolutional neural network to estimate per-voxel traversability.

more prone to failure due to sensor occlusions or image degradations [3].

Probabilistic map representations that fuse sensor readings from multiple viewpoints, e.g. 3D voxel representations, are more robust against occlusions and single instances of sensor failure. TE based on such representations is the most popular choice for long-term deployment in challenging, cluttered environments, as it allows for larger scale re-assessment and re-planning as new information is acquired by the sensors. For example, the most successful teams participating in the system track of the DARPA Subterranean challenge used such methods, as summarized in Tranzatto et al. [5]. These capable approaches assume environments to be rigid and are thus incapable of dealing with pliable vegetation. To date, no 3D voxel representations have proven fully suitable for TE in challenging vegetated environments [6], [2].

In our previous work, we demonstrated the feasibility of TE in complex vegetated environments using a 3D voxel-based representation of multiple ray statistics, color fusion and consideration of a voxel’s neighborhood. While the method showed strong results in offline-processing, it was unsuitable for real-world deployment due to high inference time. In comparison, SCNNs have shown low inference time for sparse voxel representations, which are suitable for TE estimation and scene completion in structured environments [7]. Our work leverages these findings and presents a novel TE approach suitable for real-world deployment (in terms of accuracy and inference time) in complex vegetated environments such as those shown in Fig. 1.

In this paper we propose a novel method that consists of a high-fidelity and feature-rich 3D voxel representation that leverages the structural context and sparseness of sparse

¹ QUT Centre for Robotics, Queensland University of Technology (QUT), Brisbane QLD 4000, Australia. All correspondence should be addressed to fabioadrian.ruetz@qut.edu.au

² Robotics and Autonomous Systems Group (RASG), CSIRO, Pullenvale, QLD 4069, Australia.

³ Emesent, Milton, QLD 4064, Australia.

The authors acknowledge support from the Queensland University of Technology (QUT), through the Centre for Robotics, and CSIRO Data61.

convolutional neural networks (SCNNs) to allow for rapid inference. We employ a 5-layer Unet model with three skip connections. The proposed method is thoroughly evaluated on a challenging real-world data set and is shown to significantly outperform state-of-the-art methods (0.59 vs. 0.39 MCC score at 0.1m voxel resolution) in challenging scenes and to generalize to unseen environments. The small model size (approximately 2 million parameters [17 MB] per model) allows for quick training and deployment. Furthermore, the dataset size required for training is economical and the method is trained exclusively on real-world data.

To ensure high-quality data for our learning approach, a novel probabilistic method is also introduced for accurate traversability labeling, combining self-supervised labels from previous robot experience with hand-labeled data. The robot itself is treated as an observation model to generate probabilistic collision maps from its experience moving through, and interacting with, the environment. This data is further fused with hand-labeled data, avoiding potential discretization errors that arise from commonly used heuristics found in current approaches [2], [8]. Furthermore, we present a novel practical method to quantify the estimator sensitivity to information quality. It quantifies potential performance degradation that can occur whilst the robot is exploring its environment. This factor is not addressed in the current TE literature. Lastly, we open source our novel data set containing the features and voxel labels generated by our labeling method. We believe nothing comparable is currently available.

II. RELATED WORK

Traditionally, Traversability Estimation (TE) is based on geometric features and heuristics, which perform well in structured and unstructured environments with little clutter or vegetation [9]. However, extended geometric and alternative approaches are necessary to safely navigate in more complex environments with denser vegetation. These methods are defined by the underlying representations they use and range from single images to 3D probabilistic maps.

RGB-D and image-based methods can either use single shots or data aggregation methods to generate feasible paths from a single viewpoint with high accuracy in traversability assessment [1], [10], but suffer from reliability issues on sensor readings degradation [1].

Late-fusion methods combine separate representations (e.g. 2.5D height map plus a semantic map) to generate a 2D cost or risk map. [11] fuses semantic and spatial cost maps for high-speed off-road driving using stereo-vision, emphasizing fast inference time at the cost of fidelity.

Regressing physical properties as traversability proxy is uncommon. [12] estimates grass pliability using a force sensor and a neural network. [4] assesses terrain roughness by evaluating image modalities and recent force-torque readings from the feet of a quadruped projected into the image. Lastly, [13] combines a semantic map with a robot’s simulated velocities to estimate the resistance to traversal, which requires a high-fidelity model of the robotic platform and suffers from the reality gap during field deployment.

Geometric TE methods rely on lidar-only or ray-based features, such as permeability (the probability of a ray passing through a voxel), which show promise but underperform in real-world systems [14]. These features primarily rely on point cloud statistics, resulting in high computational costs and large discretization trade-offs. Modern approaches suffer from the same issue [15]. Octomap [16] introduced a 3D voxel grid that addressed the memory and computational issues but the discretization and lack of salient features make it unsuitable for TE in cluttered, vegetated environments. [17] introduces occupancy representation with sub-voxel resolution, addressing the issue of clutter but lacking salient features. Normal Distributed Transform Traversability Map (NDT-TM) [2] expanded this by introducing salient ray features, intensity, permeability, roughness, and slope angle to estimate TE for low vegetated environments at 0.4m voxel resolution. In our prior work [8], we further developed this probabilistic map by fusing multi-return, color, and adjacency features into the map representation. This allows us to assess traversability in challenging vegetated environments for post-processed maps [8] at higher resolutions (0.1m). [7] demonstrates TE in complex geometric environments for a system trained in simulation using 3D occupancy with the equivalent real-world experience of 57 years. The authors define traversability as the success probability of traversing the environment by simulating similar start and goal states with minor random variations. They rely on the pure occupancy state of each voxel (i.e., only geometric information) and its surroundings to assess TE for state transition with different orientations. In this paper we build on these findings by leveraging the rich probabilistic map representation from our prior work with the SCNN’s ability to incorporate environmental context. Our work further differentiates itself from the earlier works by only using a limited amount of real-world data in combination with robot experience. Our proposed method is suitable for real-world deployment.

An aspect often neglected in the TE literature is the generation of accurately labeled data. This is significant as current simulations do not offer enough physical or perceptual accuracy to replace real-world data gathering. A popular method involves utilizing robot experience, namely “Learning from Experience” (LfE), by associating the robot’s state with sensory data to produce high-quality ground truth data [4], [2], [1]. For classification approaches, the positive case (traversable) can be easily obtained. Gathering non-traversable examples can be hazardous and costly, potentially damaging the robot. Hence, the use of manual or heuristics labeling is common to generate NT examples. However, this can lead to poorly labeled NT data due to heuristics or human bias. We address these issues by presenting a novel approach that combines hand-labels with robot experience in a probabilistic fashion.

III. METHODOLOGY

A. Problem Description and Definitions

We represent the environment with a voxel map \mathbf{M} – non-overlapping 3D box volumes where information about

each voxel is stored in layers. Voxel data are updated for every observation that interacts with a cell (such as a laser beam passing through or ending in the voxel). A voxel $m_i \in \mathbf{M}$ is considered to have a true binary traversability state $s_{te}(m_i) \in \{T, NT\}$, either traversable ($T = 1$, positive class), or non-traversable ($NT = 0$, negative class). The goal of the mapping process is to estimate the state of each voxel based on observations, and the current map is passed to the estimator whenever inference is required. We train an SCNN estimator using supervised learning techniques. During deployment, we rely on deep ensembles to predict the traversability probability as the mean of predictions from ten independently-trained SCNNs, since this has been shown to increase robustness and generalization performance [18].

To capture sub-resolution features, each voxel m_i contains a 3D multi-variate Gaussian distribution with probabilistic occupancy information, known as normal distributions transform occupancy maps (NDT-OM) [17]. In addition to occupancy and NDT features, we maintain statistics considering rays passing close to the distribution inside the voxel, multi-return statistics, and intensity statistics as well as robust color fusion [8]. We leverage the computation- and memory-efficient open-source occupancy homogeneous map (OHM) library [19] to continuously fuse the large amounts of lidar and RGB information into this probabilistic voxel representation at high frequency.

Final maps that utilize all data from a particular experiment are generated using a post-processing procedure. First, robot pose estimates and surfel locations are optimized using the Wildcat inertial-lidar SLAM algorithm [20]. The resulting frame-aligned trajectory and lidar ray observations are passed to the OHM mapping framework to generate feature statistics in a sparse voxelised map representation referred to as an ohm-map. This post-processing pipeline can process long deployments and fuse data on large-scale maps without needing to release or remove any data.

For probabilistic voxel representations, it is important to gather sufficient information such that the underlying statistics in each voxel represent the environment adequately and the estimator is able to make accurate predictions. We refer to this as the “information quality” of a voxel. Since each voxel and feature statistic are assumed to be independent, a quantitative formulation of a joint measure of uncertainty or entropy has not been shown. For data-driven and learning-based TE approaches, combining independent features is a common practice. This work does not aim to quantify the information quality but rather understand how sensitive an estimator is to it, by examining classification performance in an exploration setting, where information is sequentially received and processed.

We use temporal slices of our online version of the mapping framework to evaluate the sensitivity to information quality. We extract the map and its statistics at certain time steps t of an experiment, using only data fused into the map up to t . Each temporal slice only maintains a fixed size, containing local statistics around the robot due to memory and computational constraints for real-time deployment. In

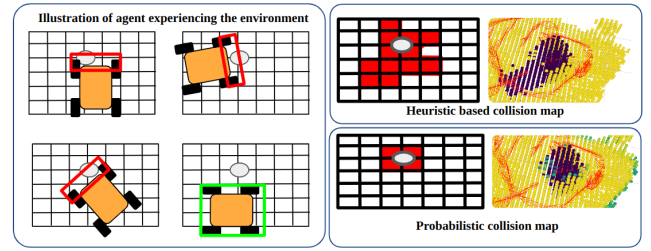


Fig. 2. Left: Illustration of instances of a robot traversing or colliding with environmental elements. The red bounds indicate the voxels that may cause the collisions, green boxes are voxels that the robot successfully traversed. Top right map: Heuristic collision map cannot override collision states, resulting in mislabeled voxels. Bottom right image: Our probabilistic collision map assess the voxel correctly as traversable. Dark purple is non-traversable, yellow traversable and green uncertain. The red arrows are discrete poses of the trajectory.

comparison to the post-processed ohm-maps the temporal slices use lidar odometry for their pose estimate, and not the global, post-processed trajectory. Therefore, these estimates suffer from drift and are locally transformed using an iterative-closest point algorithm to align each slice with the final map for calculating error statistics [21]. Some alignment error may persist between the slices and the final map, leading to the incomplete coverage statistics shown in Fig. 6.

B. Feature sets

This work uses features calculated on the ray statistics accumulated in the 3D voxel-based ohm-map. We evaluate six feature sets, each containing a different subset of features, shown in Tab. I. The sets were selected to cover a range of feature complexity in terms of sensor capabilities, saliency and computational effort to calculate.

The occupancy feature set F_{OCC} represents the simplest case of probabilistic map representation. The sub-voxel occupancy features f_{OCC} are derived from NDT-OM [17]. The F_{RGBO} set additionally includes voxel color information f_{RGB} , data that could be generated using an RGB-D camera, which are widely used in the robotics community.

The remaining sets use additional lidar information. The work in [2] introduced the intensity mean and variance features f_I , permeability (rate at which a ray is expected to pass through the 3D Gaussian distribution) ρ , inclination of a best-fit slope in a voxel θ , and roughness R . The eigenvalue features $f_{EV} = \{\lambda_L, \lambda_P, \lambda_S\}$ aim to capture how similar the point distributions are to a linear λ_L , planar λ_P or spherical λ_S element [14], but are relatively expensive to calculate. The multi-return features f_{MR} are available from some lidars and occur when the lidar receives multiple return values from a single transmitted pulse [8].

The $F_{LIDAR-BASIC}$ set uses only basic lidar information, and was chosen due to its low computational effort by avoiding eigenvalue decomposition. Since the hit-miss update of NDT-OM overlaps with the permeability update calculation, it can be added at a minimal computational cost. The $F_{LIDAR-FULL}$ set combines all lidar features, shown to contain expressive point cloud and voxel-based statistics [14], [15]. The F_{NDT} set was proposed in [2] and aims to minimize the number and redundancies of features. Finally, F_{FTM}

TABLE I
FEATURE SET OVERVIEW.

Feature set	f_{OCC}	f_{RGB}	f_I	ρ	θ	R	f_{EV}	f_{MR}
F_{OCC}	✓							
F_{RGB}	✓	✓						
$F_{LIDAR-BASIC}$	✓		✓	✓				
$F_{LIDAR-FULL}$	✓		✓	✓	✓	✓	✓	✓
F_{NDT}			✓	✓	✓	✓	✓	
F_{FTM}	✓	✓	✓	✓	✓	✓	✓	✓

uses all available features. Note that the compared support vector machine (SVM) approach (Sec. IV) includes additional adjacency information in F_{FTM} that is not required by the network as adjacency is implicitly accounted for.

C. Probabilistic collision maps for learning from experience

Any supervised data-driven approach for estimating traversability requires accurately-labeled data. We propose combining learning from robot experience (LfE) and human domain knowledge to generate our labeled data. Compared to other work, we apply a stationary binary-Bayesian filter in its log odds formulation, similar to occupancy mapping, and view the robot and its state as an observation model. A robot is manually remotely operated through a vegetated environment and its exteroceptive sensor data and pose are automatically logged. During the experiment, the robot experiences either collision-free driving or collisions, as recorded by the operator. The trajectory is used to create a labeled collision map, where each state in the trajectory at time t (defined by collision state c_t and robot pose T_t^{MR}) generates an observation for all voxels m_i that intersect with a bounding box surrounding the robot. If the robot is not in collision, all voxels intersecting the bounding box are observed as traversable. Otherwise, the voxels within the bounding box at the front of the robot and slightly beyond (0.2m) are observed as non-traversable. In the resulting collision map, each voxel contains the likelihood of being responsible for a collision $l(m_i)$, and thus also untraversable. The update in compact log-odds form is:

$$l(m_i|c_{1:t}, T_{1:t}^{MR}) = l(m_i|c_t, x_t) + l(m_i|c_{1:t-1}, T_{1:t-1}^{MR}). \quad (1)$$

The map is initialized with the hand-labeled data using fixed prior probabilities for each traversability class; empirically selected values of $p_{NT} = 0.3$ and $p_T = 0.7$. In comparison to our probabilistic approach, heuristic-based methods generally rely on conservative labeling, where recorded collision states cannot be overridden. This can lead to erroneous collision labels as shown in Fig. 2 with real-world data.

D. Network Architecture and Training Procedure

A 5-layer U-Net architecture [22] is employed for this problem, similar to [7] but without the pruning layers (visualized in Fig. 3). The resulting network is relatively small ($\sim 2M$ parameters versus standard U-Net $\sim 30M$). We use cross-entropy loss from the Minkowski Engine implementation of SCNNs [23]. To combine the different post-processed scenes or maps into a data set format suitable for training, we use an approach where the maps are split into smaller map patches of $32 \times 32 \times 32$ voxels. Each voxel appears in only one patch, and a patch requires at least $n = 150$ non-empty voxels to be

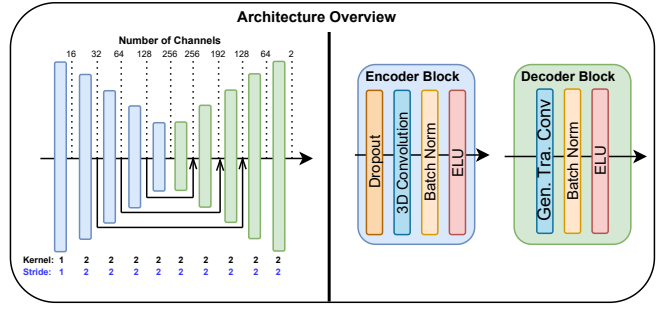


Fig. 3. Overview of the U-Net architecture used in this work. The network diagram shows the number of channels, kernel sizes, strides, and skip connections.

considered valid. These map patches are then concatenated into a single large data set. Note that the splits for training and test data are performed on a scene level.

We employ two training strategies. The first is a classical ten-fold cross-validation with a held out test scene (#9), ensuring a fair comparison against other methods. We use a 70/30 train-validation split for all cases. All features are individually scaled using zero-mean normalization, with the scaling calculated based on the training set. The second strategy is a scene-based cross-validation, where a single scene is held out and the remaining scenes are split into training-validation sets with random shuffling and data augmentation to ensure generalization. This provides a broader understanding of the ability of our method to generalize. Monte Carlo dropout is used to induce noise into the network and in testing showed higher performance and smaller variance compared to adding Gaussian noise to each feature. Geometric modifications are applied to a complete patch and include fixed angle rotation $\phi \in \{0, 90, 180, 270\}^\circ$ around the gravity-aligned axis with a uniform chance. The fixed rotation intervals are required to maintain alignment with the voxel representation. In addition, a random translation of 1-10 voxels is applied to each patch with a 50% chance.

E. Data Set

We open-sourced the data sets¹ for this work and a statistics summary can be found in Tab. II. The scenes were initially hand-labeled by an expert with domain knowledge. The data sets were augmented using the experimentally-generated collision maps, described in Sec. III-C, producing a high-quality data set. Data was collected using the tracked platform detailed in Sec. IV-A and depicted in Figs. 1, 4. Tab. II summarizes the environments and data sets by scene. The location of the scenes can be seen in the bottom right image of Fig. 2. The second column shows the total number of labeled voxels N_{labels} . Columns three to six show the percentage of labels that are traversable (T) or non-traversable (NT), and the labeling method; hand-labels (HL) or learning from experience (LfE). The seventh column shows the mean column density – the ratio of voxels containing information over the total voxels up to 1.5m above the ground. This

¹Data sets available at <https://data.csiro.au/collection/csiro:58941>

TABLE II
OVERVIEW DATA SET

Scene	N_{voxels}	T HL [%]	T LfE [%]	NT HL [%]	NT LfE [%]	Density	Dimensions [m]
# 1	86613	0.45	0.22	0.29	0.04	0.4	$18.2 \times 12.0 \times 3.9$
# 2	88410	0.6	0.2	0.16	0.03	0.25	$17.5 \times 16.0 \times 3.5$
# 3	146121	0.66	0.32	0.02	0	0.3	$24.6 \times 15.7 \times 4.3$
# 4	282197	0.62	0.38	0	0	0.15	$30.0 \times 26.0 \times 3.4$
# 5	113288	0.53	0.47	0	0	0.2	$23.3 \times 17.9 \times 2.5$
# 6	73073	0.26	0.18	0.44	0.12	0.15	$13.3 \times 15.0 \times 1.9$
# 7	120442	0.47	0.22	0.26	0.04	0.24	$25.1 \times 18.8 \times 1.8$
# 8	102560	0.48	0.09	0.4	0.02	0.19	$14.8 \times 17.7 \times 3.0$
# 9	88410	0.6	0.2	0.16	0.03	0.25	$17.5 \times 16.0 \times 3.5$



Fig. 4. Top far left: QCAT testing facility in Queensland, Australia and the approximate locations where the data sets were gathered. [1] and [2]: robot in forest environments from the robot and external viewpoint, respectively. [3] and [4]: robot in tall grass with some large trees. [7]: environment with a mixture of small to medium trees and patchy vegetation.

aims to measure the vegetation density in the area of interest. Lastly, we provide the dimensions of the bounding volume for each scene in x, y, z gravity-aligned coordinate frames.

IV. EXPERIMENTS AND RESULTS

We begin with an overview of the data set and implementation details. We then provide two experimental evaluations on the post-processed data and compare against SOTA methods. Next we analyze the estimator’s sensitivity to information quality. Finally, we provide qualitative examples of our method in unseen, real-world environments. Throughout this work, we evaluate using the Matthews correlation coefficient (MCC) score which effectively addresses high-class imbalance. MCC computes the correlation coefficient between predicted and true labels, treating classes as binary random variables, making it a descriptive metric for highly imbalanced data sets [24]. The F1-score is also provided since it is a classical comparative metric.

A. Platform and Implementation Details

The robot we used for data collection (Dynamic Traced Robot (DTR)), is a 35 kg tracked vehicle equipped with a sensory pack containing IMU, a rotating Velodyne VLP-16 angled at 45° and four RGB cameras. The lidar is mounted on top of the robot and performs a full revolution at 2Hz. Fig.1 depicts the vehicle in an environment representative of this work. Further details on the platform can be found in [8].

The network’s learning and noise parameters were determined by scene-based cross-validation using the ADAM optimizer. The parameters were optimized to maximize the MMC score and minimize the variance between each fold. They were set as follows: learning rate $l_r = 10^{-4}$, weight decay $w = 9 \times 10^{-4}$, batch size $b = 48$, early stopping patience $es = 5$ and maximum epoch number $epoch_{max} = 250$, with average convergence between 50–100

TABLE III
CLASSIFICATION PERFORMANCE ACROSS ESTIMATOR TYPE, VOXEL SIZE (VS), AND FEATURE SET USING TEN-FOLD CROSS-VALIDATION ON AN UNSEEN TEST (SORTED BY DECREASING MCC VALUES).

Estimator	Feature Set	vs [m]	MCC ($\mu \pm \sigma$)	F1-Score ($\mu \pm \sigma$)
SCNN	F_{NDT}	0.1	0.58 ± 0.04	0.78 ± 0.02
SCNN	$F_{LIDAR-BASIC}$	0.1	0.55 ± 0.05	0.77 ± 0.03
SCNN	F_{FTM}	0.1	0.54 ± 0.04	0.75 ± 0.03
SCNN	F_{OCC}	0.1	0.54 ± 0.05	0.75 ± 0.04
SCNN	F_{RGBO}	0.1	0.50 ± 0.06	0.72 ± 0.04
SCNN	$F_{LIDAR-FULL}$	0.1	0.48 ± 0.05	0.71 ± 0.04
SVM	F_{FTM}	0.1	0.39 ± 0.00	0.60 ± 0.00
SVM	F_{NDT}	0.1	0.35 ± 0.00	0.58 ± 0.00
SCNN	F_{NDT}	0.2	0.52 ± 0.03	0.75 ± 0.02
SCNN	$F_{LIDAR-BASIC}$	0.2	0.49 ± 0.05	0.74 ± 0.03
SVM	F_{FTM}	0.2	0.48 ± 0.00	0.67 ± 0.00
SCNN	F_{FTM}	0.2	0.47 ± 0.04	0.71 ± 0.03
SCNN	$F_{LIDAR-FULL}$	0.2	0.45 ± 0.04	0.71 ± 0.02
SCNN	F_{RGBO}	0.2	0.43 ± 0.03	0.68 ± 0.02
SVM	F_{NDT}	0.2	0.41 ± 0.00	0.62 ± 0.00
SCNN	F_{OCC}	0.2	0.39 ± 0.05	0.68 ± 0.04

epochs. Training time was 3.1 minutes/model on average on a computer equipped with an NVIDIA GeForce RTX 3090, 32 GB of system memory, and an Intel Core i7-11700K processor.

We claim our method as real-time capable. OHM [19] runs at 5Hz for a volume ($30 \times 30 \times 10 \text{m}$) for our systems. Our method’s inference time was observed to be 200-420ms for the accompanying video.

B. Traversability estimation evaluation

1) *Comparison to SOTA methods*: Our set of experiments investigates the benefits of using an SCNN compared to classical machine learning methods in [2] and our prior work [8] using SVMs. Our method is trained using 10-fold cross-validation, as discussed in Sec. III-A and, due to the methods requiring different training strategies, they are compared on a novel, unseen test set.

Results are shown in Tab. III for voxel sizes (vs) of 0.1m and 0.2m. The table shows that all SCNN feature sets significantly outperform SOTA methods in 0.1m, with an MCC score of 0.58 vs. 0.39, a 49% performance increase. Unexpectedly, using the pure geometric feature set F_{OCC} yields comparable performance to the full feature set F_{FTM} but performs poorly at lower resolutions. For vs 0.2m two lidar-only feature sets outperform our prior work, whilst the full feature sets F_{FTM} method is comparable when using SVM or SCNN performance-wise.

Fig. 5 A and E show the RGB fusion and the ground truth of the test set at 0.1m voxel resolution. The test set includes both open space and varying vegetation density levels. Significant vegetation can be seen near the ground, which the robot must consider to navigate safely. Comparing the MCC scores of Tab. III to Tab. IV indicates that the test scene can be considered challenging from a traversability classification standpoint.

The top row (B-D), shows the traversability probability for the SVM F_{FTM} , SCNN F_{FTM} and SCNN F_{RGBO} models. An ensemble approach is employed for the SCNN models, to compute a mean prediction probability using the models from the 10-cross-fold validation. The second row (F-G) shows the classification results of each method

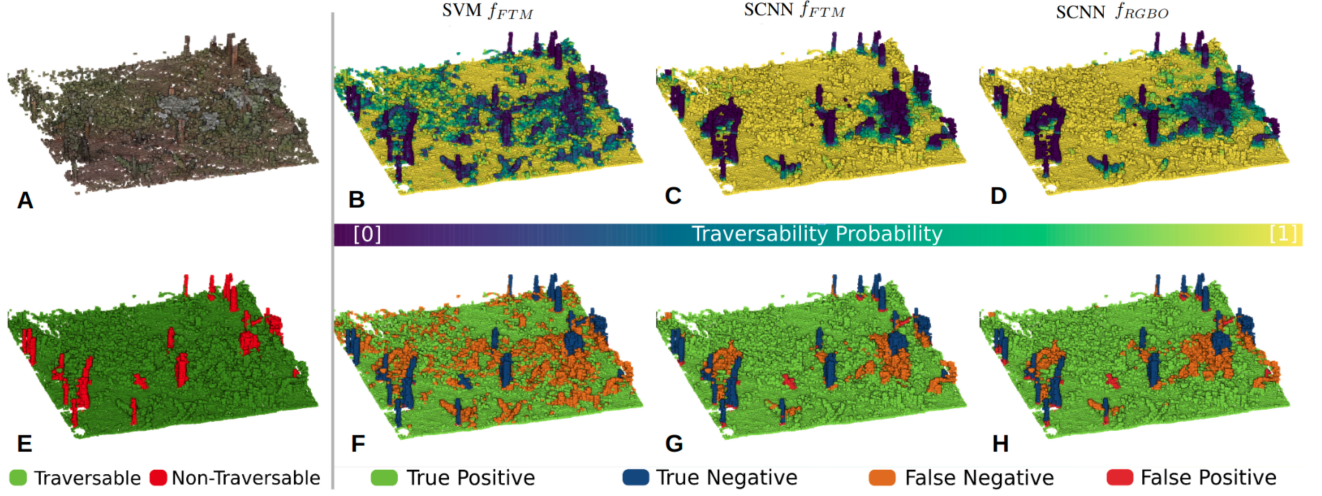


Fig. 5. Left column: **A** RGB voxel cloud and **(E)** ground truth labels of the test scene. Second column: **B** traversability probability of our previous work SVM f_{FTM} and **F** classification results compared to the ground truth. Green is true positive (TP), blue is true negative (TN), orange is false negative (FN) and red is false positive (FP). The third and fourth columns show the classification probability for f_{FTM} (**C**, **G**) and f_{RGBO} feature set for the SCNN estimator (**D**, **H**).

compared to the ground truth data set. The SVM method (column 2) shows high certainty and accuracy for large, non-traversable elements such as tree trunks. In addition, it successfully detected a small hidden tree trunk within the vegetation where other SCNN models failed. However, it shows high uncertainty, indicated by the green hue, in the vast areas with low-medium vegetation emerging from the ground that are wrongly classified as non-traversable (FN), rendering large areas of the map non-traversable, as seen in sub-image G. All SCNN models exhibit comparable high accuracy, with minor quantitative variations and some qualitative distinctions. In general, they correctly assessed the TE for large elements such as trees and the light to medium vegetation up to a meter above the ground. However, they all wrongly classified the foot of many trees as traversable (FP). The two mainly geometric feature sets, F_{OCC} and F_{RGBO} , struggle with this in particular, which can be clearly observed in the accompanying video. However, the majority of the tree is correctly classified as non-traversable. The other main difference between the SCNN models is the traversal probability in the middle patch between the three trees. The geometric models consistently misclassified dense vegetation with high certainty, whereas the other methods had either correctly classified the vegetation or the traversal probabilities were less certain.

2) *Evaluation on scene-based cross-fold evaluation:* This experiment shows our method’s ability to generalize for each feature combination. Overall, this experiment provides a clear understanding of how well the estimators can generalize in different scenes and provides an indication of their expected performance in similar environments. Table IV shows the results of a cross-fold validation over six of the nine scenes. Two models were excluded due to the absence of negative examples (NT), which would skew the results. The last scene

TABLE IV
SCENE-BASED CROSS-VALIDATION FOR DIFFERENT FEATURE SETS AND RESOLUTIONS, SORTED BY DECREASING MCC VALUES.

Feature Set	vs [m]	MCC ($\mu \pm \sigma$)	F1-Score ($\mu \pm \sigma$)
$F_{LIDAR-BASIC}$	0.1	0.74 ± 0.07	0.86 ± 0.03
F_{OCC}	0.1	0.72 ± 0.07	0.86 ± 0.03
F_{NDT}	0.1	0.70 ± 0.10	0.84 ± 0.06
F_{FTM}	0.1	0.69 ± 0.13	0.83 ± 0.08
$F_{LIDAR-FULL}$	0.1	0.68 ± 0.10	0.83 ± 0.06
F_{RGBO}	0.1	0.67 ± 0.12	0.82 ± 0.07
F_{FTM}	0.2	0.71 ± 0.06	0.85 ± 0.03
$F_{LIDAR-FULL}$	0.2	0.68 ± 0.07	0.83 ± 0.04
$F_{LIDAR-BASIC}$	0.2	0.68 ± 0.07	0.83 ± 0.04
F_{OCC}	0.2	0.68 ± 0.07	0.83 ± 0.04
F_{NDT}	0.2	0.67 ± 0.09	0.82 ± 0.05
F_{RGBO}	0.2	0.64 ± 0.08	0.81 ± 0.05

is reserved as the hold-out test set, as discussed above.

We note that for the 0.1m voxel resolution, the $F_{LIDAR-BASIC}$ feature set and the pure occupancy F_{OCC} showed the strongest performance. The other feature sets are similar in performance close to 0.69 MCC score. At 0.2m voxel resolution, the full feature set F_{FTM} outperforms any other feature set. Pure lidar and occupancy measures are close, whereas the occupancy with RGB and NDT features are less informative. Note that all feature sets at vs 0.1m containing F_{RGB} have a significantly higher spread of their performance over scenes, as can be seen by the higher standard deviation.

C. Analysis of Estimator’s Sensitivity to Information Quality

This experiment demonstrates a method for evaluating the sensitivity of a TE model to information quality. This enables a quantitative understanding of the consequences and TE performance implications of training on post-processed data and deploying in real-world scenarios. In field deployments, information is received sequentially as the robot explores the environment. To simulate this, we extract maps at discrete time intervals (ohm-scans) representing temporal map slices.

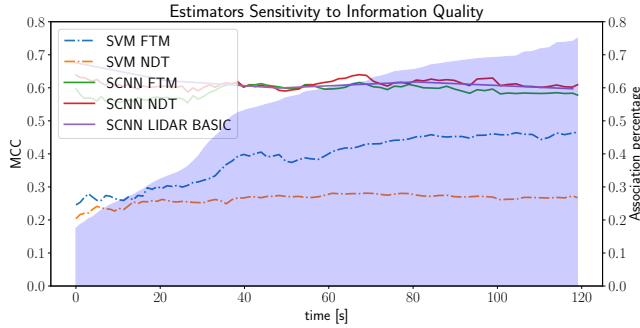


Fig. 6. Classification performance of a system at time t on an unobserved environment. It compares our method (solid lines) using different feature sets with SOTA methods (dotted lines). The blue background shows the association percentage between the ohm-scan and ground-truth map, a proxy for the amount of the scene explored.

We compare the estimator’s prediction of the ohm-scans against the ground-truth map for an unobserved test scene (#9). These results are compared against the results in Tab. III, since they are the same test scene. The plot Fig. 6 shows the performance of TE estimators. For the SCNN models, there is little to no performance drop and the prediction accuracy is nearly constant over time. This indicates a primary reliance on the structure of the environment for the traversability assessment. In addition, the performance is close to the performance found for evaluation using post-processed data which indicates a good generalization (~ 0.6 MCC score) from the previous experiment. Quantitatively, there are no significant performance differences between feature sets used, but qualitatively, we can see some in Figs. 7. The SVM models with the F_{FTM} and F_{NDT} show strong sensitivity to information quality, resulting in degraded performance. In the case of F_{FTM} , the performance increases continuously until it reaches a steady state. This indicates that this method heavily relies on features that require a significant amount of information to be gathered until it can accurately estimate the traversability. Therefore, it struggles with real-world deployment until large parts of the scenes are explored. Once the information quality is sufficient the SVM F_{FTM} achieves similar classification performance as in the post-processed data experiments indicating that it does generalize. In the case of SVM F_{NDT} it performs worse than in the comparable post-processed experiment. This indicates that there are combinations of feature sets and estimators that are not well-suited for real-world deployment. The blue plot shows the association of an ohm-scan to the ground truth map. It approximates how much of the scene has been observed at least once; the percentage grows continuously until reaching a steady state. As indicated in Sec. III-A, the differences can be explained by the odometry and SLAM trajectories alignment and removal of unclear elements during labeling. Our novel method is clearly less sensitive to information quality than the SOTA methods. Secondly, this evaluation is practical to characterize and gauge the suitability of a TE method for exploration and thus robot deployment.

D. Qualitative Evaluation

Fig. 7 shows the TE classification for an exploration setting. A larger platform with the same sensor configuration but a different lidar spin rate traveled through a forest environment remotely controlled by an operator, shown by the birds-eye view top left. Image A shows the TE probability 10 seconds after the mission starts and B approximately ten seconds later. This indicates how a single viewpoint is limiting. C shows the robot driving through tall grass, thereby obstructing almost all the environment except the patch close to the robot. D and E show scenes further into the forest where dense foliage is less prominent, but many thin and tall small trees are frequent. In all the scenes the robot position is indicated by the RGB axes.

V. DISCUSSION

The ability of the SCNN to leverage pure geometric information is impressive. Our results show that the SCNN at our higher voxel resolutions heavily relies on contextual geometric information for TE. Furthermore, this enables a reduction in the number of features and sensor modalities used with only minor loss in performance. For example, our method can perform TE in complex environments using just a single lidar, significantly reducing technical and computational complexity. Quantitatively the summary statistics of the feature sets (other than occupancy) show marginal performance gains. In the accompanying video we show the qualitative differences that result from using different feature sets. For example, we observed that additional features help to discriminate vegetation close to the ground. This was particularly notable where lower parts of tree trunks were being misclassified. The additional features provide a further gradual boundary between T and NT elements which is most commonly observed for leafy elements (e.g. bushes). In the summary statistics, this is not obvious as the number of voxels affected is comparatively low. Over-reliance on geometric structure compared to other features can be potentially limiting when the geometry is ambiguous or geometric information cannot be acquired (e.g., lidar occlusion in high, dense grass). However, this is not a major concern for our method, as the underlying probabilistic map enables a planner to prioritize safer paths, even if they are longer, by avoiding particularly challenging areas.

Another key benefit of the method is its practicality. The low computational requirements, training time, and training data allow this method to be broadly applicable. We believe it is suitable for any scenarios involving vegetation, not just dense forest navigation.

In practice, using a combination of features from different representations is typical for learning-based TE methods. Quantifying joint uncertainty or entropy of all the features/statistics of a single voxel is often not feasible. Hence, the presented evaluation is a practical method to assess the TE’s performance whilst exploring new areas.

Color information has been reported as a powerful feature for classification [4], [1]. However, we found that color features can degrade classification performance in some cases,

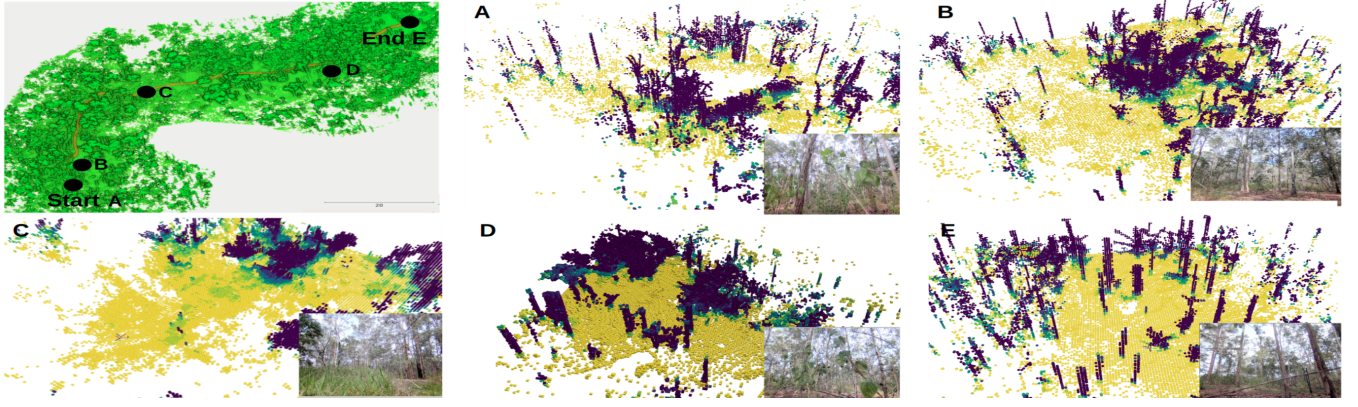


Fig. 7. Qualitative examples of a trajectory performed in an unknown environment with. The left image shows a bird's eye view of the scene with traversability probability results on a post-processed scene. A different sensor-pack was used, with the same sensor configuration but double the spin-rate.

as similarly reported by Bradley et al. [3]. Common issues include sensor misalignment, camera occlusions, or a voxel containing multiple colors.

The strong geometric reliance also raises a question about the necessity of feature-rich probabilistic maps; how complex and computationally expensive they need to be to achieve safe navigation, which is often referred to as “perceptual economy”. At a vs of 0.2m, we noted that more complex features started to play a more significant role in the estimation, whereas at 0.1m geometry is dominant. Hence, how to increase or decrease the importance of geometry or features for a given vs remains an interesting question.

VI. CONCLUSION

We proposed a real-time capable TE pipeline that outperforms SOTA methods in accurately predicting voxel-based traversability in dense vegetation. Our approach leverages the environmental context of the SCNN, reducing the complexity and number of salient features required with little performance loss. Trained solely on real-world data, our method is cost-effective in terms of training data and time. Through a comprehensive evaluation, we demonstrated the performance and generalization capabilities of our TE method, including a novel analysis of sensitivity to information quality.

Future work will involve exploring behavioral strategies, environmental semantics and incorporating voxel information with out-of-distribution detection. This combination could enable targeted active learning, where the robot purposely interacts and learns in new environments.

REFERENCES

- [1] G. Kahn, P. Abbeel, and S. Levine, “BADGR: An autonomous self-supervised learning-based navigation system,” *IEEE RAL*, vol. 6, no. 2, 2021.
- [2] J. Ahtiainen, T. Stoyanov, and J. Saarinen, “Normal distributions transform traversability maps: Lidar-only approach for traversability mapping in outdoor environments,” *Journal of Field Robotics*, vol. 34, no. 3, 2017.
- [3] D. M. Bradley, J. K. Chang, D. Silver et al., “Scene understanding for a high-mobility walking robot,” in *IROS*, 2015.
- [4] L. Wellhausen, A. Dosovitskiy, R. Ranftl et al., “Where should I walk? predicting terrain properties from images via Self-Supervised learning,” *IEEE RAL*, vol. 4, no. 2, 2019.
- [5] M. Tranzatto, F. Mascari, L. Bernreiter et al., “Cerberus: Autonomous legged and aerial robotic exploration in the tunnel and urban circuits of the darpa subterranean challenge,” (*JFR accepted*) *arXiv preprint arXiv:2201.07067*, 2022.
- [6] D. Maturana, P.-W. Chou, M. Uenoyama, and S. Scherer, “Real-time semantic mapping for autonomous off-road navigation,” in *Field and Service Robotics*. Springer, 2018, pp. 335–350.
- [7] J. Frey, D. Hoeller, S. Khattak, and M. Hutter, “Locomotion policy guided traversability learning using volumetric representations of complex environments,” in *IROS*, 2022.
- [8] F. Ruetz, P. Borges, N. Suenderhauf, E. Hernández, and T. Peynot, “Forest traversability mapping (FTM): Traversability estimation using 3D voxel-based normal distributed transform to enable forest navigation,” in *IROS*, 2022.
- [9] P. Papadakis, “Terrain traversability analysis methods for unmanned ground vehicles: A survey,” *Engineering Applications of Artificial Intelligence*, vol. 26, no. 4, 2013.
- [10] S. Siva, M. Wigness, J. G. Rogers et al., “NAUTS: Negotiation for adaptation to unstructured terrain surfaces,” in *IROS*, 2022.
- [11] X. Meng, N. Hatch, A. Lambert et al., “TerrainNet: Visual modeling of complex terrain for high-speed, off-road navigation,” *arXiv preprint arXiv:2303.15771*, 2023.
- [12] C. Ordóñez, R. Alicea, B. Rothrock et al., “Characterization and traversal of pliable vegetation for robot navigation,” in *Proceedings of the 2018 International Symposium on Experimental Robotics*. Springer, 2020, pp. 293–304.
- [13] X. Cai, M. Everett, J. Fink, and J. P. How, “Risk-aware off-road navigation via a learned speed distribution map,” in *IROS*, 2022.
- [14] J.-F. Lalonde, N. Vandapel, D. F. Huber, and M. Hebert, “Natural terrain classification using three-dimensional lidar data for ground robot mobility,” *Journal of field robotics*, vol. 23, no. 10, 2006.
- [15] P. Krüsi, P. Furgale, M. Bosse, and R. Siegwart, “Driving on point clouds: Motion planning, trajectory optimization, and terrain assessment in generic nonplanar environments,” *Journal of Field Robotics*, vol. 34, no. 5, 2017.
- [16] A. Hornung, K. M. Wurm, M. Bennewitz, C. Stachniss, and W. Burgard, “OctoMap: An efficient probabilistic 3d mapping framework based on octrees,” *Autonomous robots*, vol. 34, pp. 189–206, 2013.
- [17] J. Saarinen, H. Andreasson, T. Stoyanov et al., “Normal distributions transform occupancy maps: Application to large-scale online 3d mapping,” in *ICRA*, 2013.
- [18] D. Opitz and R. Maclin, “Popular ensemble methods: An empirical study,” *Journal of artificial intelligence research*, vol. 11, pp. 169–198, 1999.
- [19] K. Stepanas, J. Williams, E. Hernández, F. Ruetz, and T. Hines, “OHM: GPU based occupancy map generation,” *IEEE RAL*, vol. 7, no. 4, 2022.
- [20] M. Ramezani, K. Khosoussi, G. Catt et al., “Wildcat: Online continuous-time 3D lidar-inertial SLAM,” *arXiv preprint arXiv:2205.12595*, 2022.
- [21] Y. Chen and G. Medioni, “Object modelling by registration of multiple range images,” *Image and vision computing*, vol. 10, no. 3, 1992.
- [22] O. Ronneberger, P. Fischer, and T. Brox, “U-net: Convolutional networks for biomedical image segmentation,” in *MICCAI*, 2015.
- [23] C. Choy, J. Gwak, and S. Savarese, “4D spatio-temporal convnets: Minkowski convolutional neural networks,” in *IEEE CVPR*, 2019.

- [24] H. Cramér, *Mathematical methods of statistics*. Princeton university press, 1999, vol. 26.